Vol. 30 • No. 18 • May 3 • 2018

www.advmat.de

ADVANCED MATERIALS

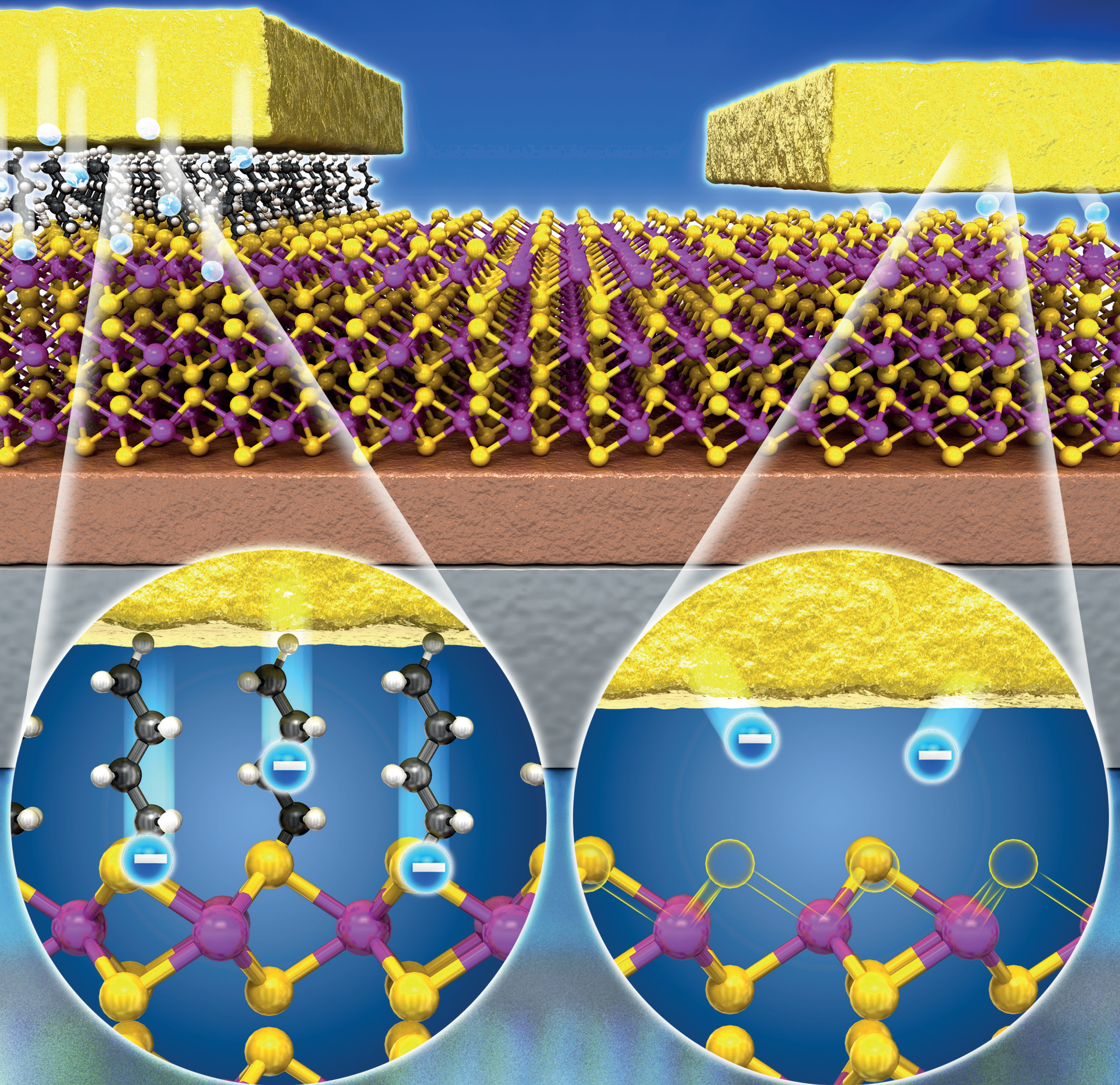

WILEY-VCH

ADVANCED MATERIALS
www.advmat.de

Contact-Engineered Electrical Properties of MoS_2 Field-Effect Transistors via Selectively Deposited Thiol-Molecules

Kyungjune Cho, Jinsu Pak, Jae-Keun Kim, Keehoon Kang, Tae-Young Kim, Jiwon Shin, Barbara Yuri Choi, Seungjun Chung, and Takhee Lee**

Although 2D molybdenum disulfide (MoS_2) has gained much attention due to its unique electrical and optical properties, the limited electrical contact to 2D semiconductors still impedes the realization of high-performance 2D MoS_2-based devices. In this regard, many studies have been conducted to improve the carrier-injection properties by inserting functional paths, such as graphene or hexagonal boron nitride, between the electrodes and 2D semiconductors. The reported strategies, however, require relatively time-consuming and low-yield transfer processes on sub-micrometer MoS_2 flakes. Here, a simple contact-engineering method is suggested, introducing chemically adsorbed thiol-molecules as thin tunneling barriers between the metal electrodes and MoS_2 channels. The selectively deposited thiol-molecules via the vapor-deposition process provide additional tunneling paths at the contact regions, improving the carrier-injection properties with lower activation energies in MoS_2 field-effect transistors. Additionally, by inserting thiol-molecules at the only one contact region, asymmetric carrier-injection is feasible depending on the temperature and gate bias.

Molybdenum disulfide (MoS_2), widely studied as a 2D semiconducting material in the transition dichalcogenides (TMDCs) family, has unique properties including good flexibility, transparency, a tunable bandgap energy controlled by the number of layers, and spin-valley physics from the strong internal magnetic field.[1–9] Due to its fascinating characteristics, MoS_2 has received much attention for the realization of promising nanoelectronics and optoelectronics. However, delivering good contact properties between 2D semiconductors and metal electrodes is still challenging, and this is essential to achieve excellent electrical and optical performances especially in the low-operation voltage regimes. Theoretically, it is predicted that a much lower contact resistance (three orders of magnitude) in MoS_2 devices might be achieved compared to the previously reported experimental values.[10] Therefore, many research groups have proposed emerging methods to improve contact properties, for example, inserting functional layers between 2D semiconductors and electrodes,[11,12] thermal annealing at contact regions,[13] phase engineering with high-energy beam irradiation,[14] and employing graphene electrodes[15,16] low-work function metals,[17,18] or a direct chemical vapor deposition (CVD)-growth method of 2D heterostructures in lateral.[19,20] However, thermal annealing and high-energy beam irradiation may damage 2D materials, and direct CVD-growth method of lateral 2D heterostructures is difficult to define accurate junction areas between 2D materials. Therefore, more facile approach to improve the contact properties between metal electrodes and 2D semiconductors is desired for the typical 2D field-effect transistor structure.

Among these methods, introducing a thin tunneling barrier between the MoS_2 channel and electrodes is an efficient approach to improve contact properties by reducing the activation energy.[12,21,22] For example, graphene or hexagonal boron nitride (h-BN) have been vertically employed between metal contacts and 2D semiconductors as a thin tunneling barrier for the lower contact resistance.[21,22] Moreover, the use of cobalt electrodes facilitated Ohmic contact even in the extremely low temperature regime.[12] However, relatively complex, high-cost, and low-yield transfer processes were required to make vertically stacked 2D heterostructures.[11,12] Additionally, it is difficult to introduce atomically thin tunneling barriers using conventional transfer methods to the exact contact location on flake-type MoS_2 with dimensions of sub-micrometer size. Here, we demonstrate a simple strategy for inserting a thin tunneling barrier by depositing thiol-molecules between MoS_2 semiconductors and conventional metal electrodes. Vaporized thiol-molecules are chemically adsorbed on MoS_2 with covalent bonding. The inserted thiol-molecules at the contact region create additional tunneling paths, resulting in a drastically reduced activation energy; therefore, the primary injection mechanism of the contact-engineered MoS_2 field-effect transistors (FETs) changes from thermionic emission to field emission, allowing better contact properties without a temperature dependency. In addition, by defining contact regions on MoS_2 using conventional lithography, where injection engineering is desirable, a selective introduction of thiol-molecules is feasible with ≈100% yield

K. Cho, J. Pak, J.-K. Kim, Dr. K. Kang, T.-Y. Kim, J. Shin, B. Y. Choi, Prof. T. Lee
Department of Physics and Astronomy
and Institute of Applied Physics
Seoul National University
Seoul 08826, South Korea
E-mail: tlee@snu.ac.kr
Dr. S. Chung
Photoelectronic Hybrids Research Center
Korea Institute of Science and Technology
Seoul 02792, South Korea
E-mail: seungjun@kist.re.kr

DOI: 10.1002/adma.201705540

© 2018 WILEY-VCH Verlag GmbH & Co. KGaA, Weinheim

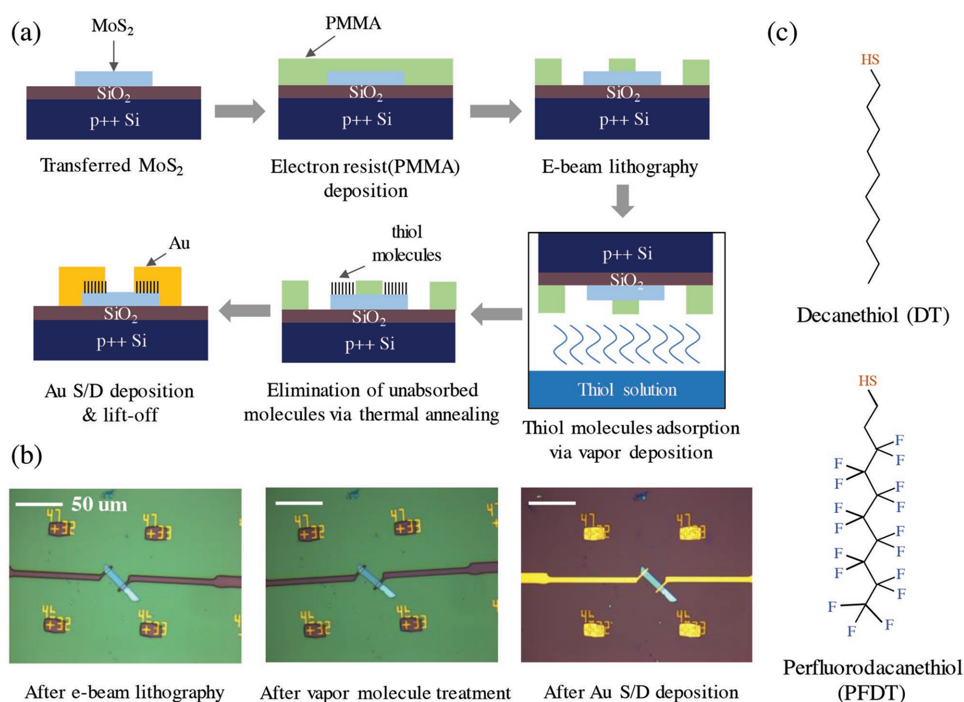

Figure 1. a) Schematic images of the device fabrication process. b) Optical images of the MoS_2 FETs during the fabrication process. c) Schematics of the decanethiol (DT) and perfluorodecanethiol (PFDT) molecule.

that could support asymmetric carrier injection in FET device applications.

Figure 1a shows the schematic images of the fabrication process of MoS_2 FETs with adsorbed thiol-molecules at the contact regions. MoS_2 flakes were transferred on a cleaned *p*-type heavily doped Si substrate (resistivity ≈5×10^{-3} Ω cm) with 270 nm thick SiO_2 with a mechanical exfoliation method. After the polymethyl methacrylate (PMMA, molecular weight of 4950 k mol^{-1}, 11% dissolved in anisole) electron resist polymer was spin-coated on the MoS_2 channel layer, the source/drain (S/D) patterns were defined using an electron beam lithography system (JSM-6510, JEOL). In addition, we deposited thiol-molecules (decanethiol or perfluorodecanethiol) via a vapor deposition method on the exposed contact region of the MoS_2 flake. Thiol-molecules are chemically adsorbed at the sulfur vacancies of MoS_2 by generating a covalent bond with Mo.[23–28] In general, functional molecules have been deposited by dipping MoS_2 samples into thiol-based solution. However, this approach requires a long duration, and the PMMA barrier patterns used to define the S/D electrodes are easily damaged by the thiol solution (Figure S1, Supporting Information). Therefore, we employed a vapor deposition method that did not destroy the PMMA patterns and allowed a selective deposition of the thiol-molecules on the specific MoS_2 contact regions (Figure 1b). The MoS_2 sample attached at the lid of a vial was exposed to vaporized thiol-molecules in the vial containing thiol solution. Note that the solution was heated up to 70 °C and the processes were performed in a N_2 glove box for 3 h. Then, the thiol-deposited MoS_2 sample was annealed on a 70 °C hot plate for 1 h to remove residual solvent. After the annealing process, 30 nm thick Au was deposited as S/D electrodes using an electron beam evaporating system (KVE-2004L, Korea Vacuum Tech.). The stability of deposited thiol-molecules is discussed in the Supporting Information. Figure 1b shows the optical images of the MoS_2 FETs with the aforementioned procedure. The left image of Figure 1b shows that only the contact regions of MoS_2 were exposed for the thiol-molecule deposition with the development process, and the MoS_2 channel region was protected by the PMMA layer. After the thiol-molecule vapor deposition process, the PMMA patterns were not destroyed by the thiol-molecule vapor (see the middle image of Figure 1b). After the Au deposition, the chemically adsorbed thiol-molecules were located between the Au S/D electrodes and the MoS_2 surface. The detailed fabrication process is explained in the Experimental Section. Figure 1c shows two types of thiol-molecules that are used in this study; one was decanethiol (DT) and the other was perfluorodecanethiol (PFDT). Both the DT and PFDT molecules have a similar molecular length, with 10 carbon chains that introduce similar tunneling path length for carriers; however, these molecules have an opposing electric dipole moments due to fluorides in PFDT, which may affect the Schottky barrier height. We will discuss this in detail later.

To verify that the thiol-molecules can be well adsorbed on the MoS_2 surface via the vapor deposition method, electron energy loss spectroscopy (EELS) with a high-resolution transmission electron microscope (HRTEM) (JEM-2100F, JEOL) was conducted for MoS_2 flakes without the thiol treatment ("untreated"), with DT treatment, and with PFDT treatment. **Figure 2**a shows the HRTEM cross-section image (left panel) of the contact region and the EELS results (middle panel) measured at the Au electrode (position 1), the interface between the Au electrode and the MoS_2 (position 2), and the MoS_2 layer (position 3). The magnified EELS profiles for position 2 are shown in the right panel of Figure 2a. Figure 2b,c

© 2018 WILEY-VCH Verlag GmbH & Co. KGaA, Weinheim

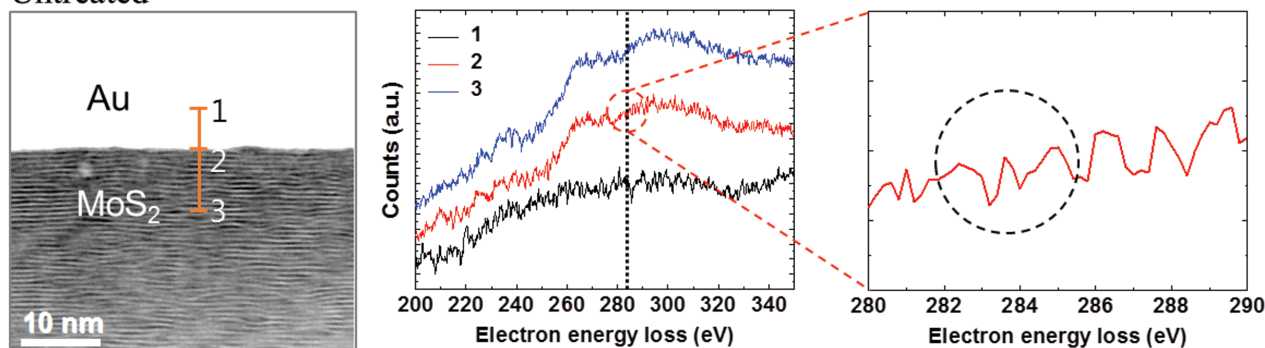

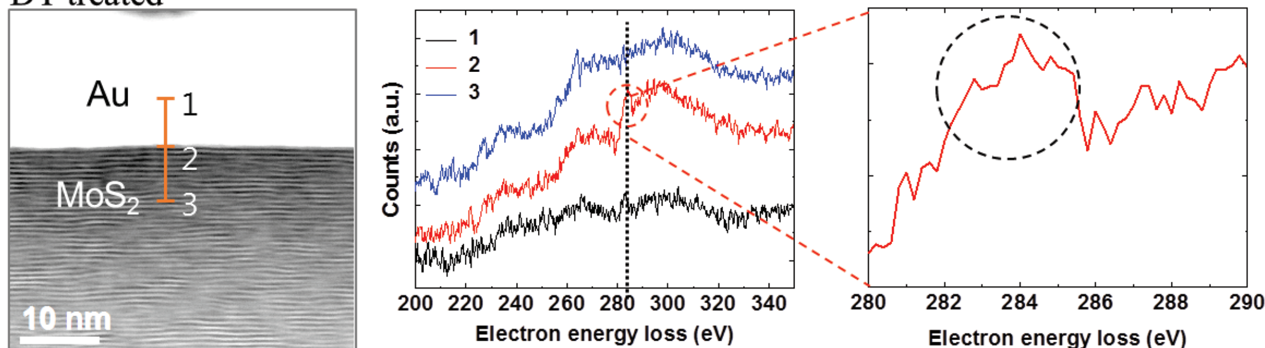

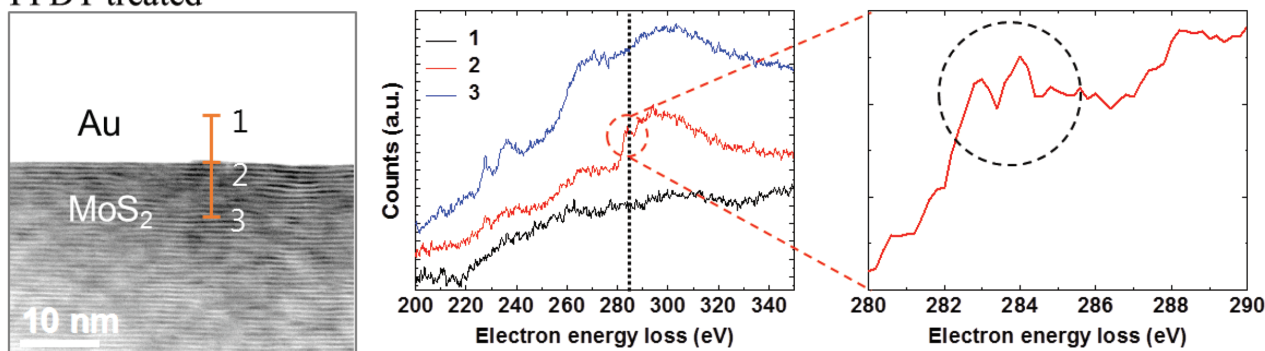

Figure 2. a) (Left) HRTEM image of untreated MoS_2 sample, (middle) EELS data along the orange line in the HRTEM image at position 1, 2, and 3 and (right) magnified EELS data at position 2. b) (Left) HRTEM image of DT-treated MoS_2 sample, (middle) EELS data along the orange line in the HRTEM image at position 1, 2, and 3 and (right) magnified EELS data at position 2. c) (Left) HRTEM image of PFDT-treated MoS_2 sample, (middle) EELS data along the orange line in the HRTEM image at position 1, 2, and 3 and (right) magnified EELS data at position 2.

shows the results of HRTEM cross-section images and EELS results for DT-treated MoS_2 and PFDT-treated MoS_2, respectively. From the magnified EELS profiles, the carbon peaks were clearly observed at the interface of DT and PFDT-treated MoS_2 at an electron energy of 284 eV, whereas they were not detected at the other positions and the interface of untreated MoS_2. Because the carbon peaks originated from the thiol-molecules adsorbed at the MoS_2 surface, these results support that thiol-molecules were inserted directly via the vapor treatment with the DT and PFDT solution between the MoS_2 layer and electrodes.

For the further investigation of the adsorbed thiol-molecules on MoS_2, X-ray photoelectron spectroscopy (XPS) (AXIS-SUPRA, KRATOS) was conducted on the prepared MoS_2 flakes. **Figure 3**a shows the optical and corresponding XPS mapping images of untreated, DT-treated, and PFDT-treated MoS_2 flakes. The positions where Mo, S, carbon (C), and fluorine (F) elements were adsorbed are indicated in blue, violet, green, and orange, respectively. As expected, in the DT- or PFDT-treated MoS_2 flakes, the C peaks were more dominantly detected compared to the untreated MoS_2 flakes. In addition, the intensity of the F peaks significantly increased on the PFDT-treated MoS_2, which is consistent with the XPS results at the binding energy of 687 eV (bottom panel, Figure 3b). In Figure 3b, the characteristic peaks of Mo and S in DT-treated MoS_2 slightly shifted to the low-energy direction, whereas those of PFDT-treated MoS_2

© 2018 WILEY-VCH Verlag GmbH & Co. KGaA, Weinheim

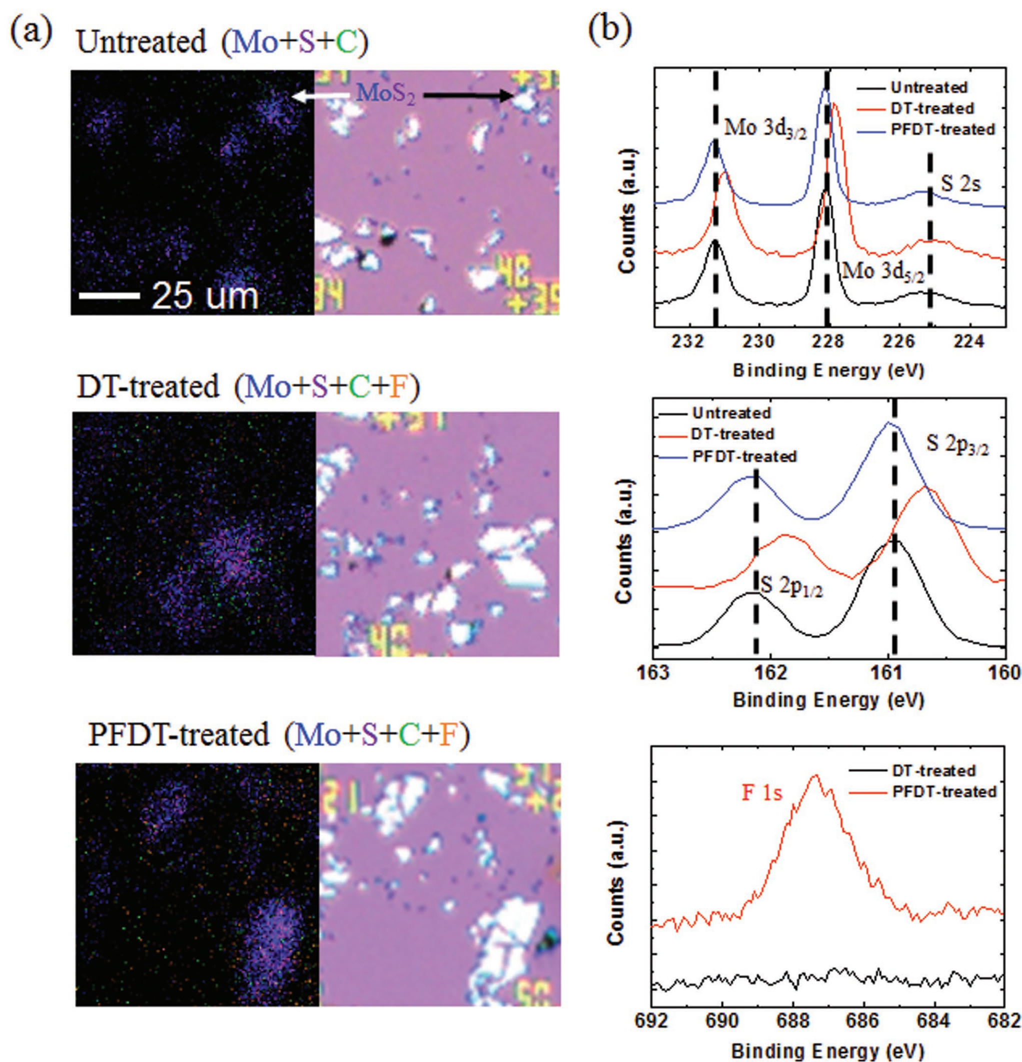

Figure 3. a) XPS mapping image and optical image of (top) untreated, (middle) PFDT-treated, and (bottom) DT-treated MoS_2. The blue dots are the positions where the Mo peak was observed in XPS, purple dots represent S, green dot represents C, and orange dot represents F. b) XPS data of untreated and thiol-treated MoS_2.

shifted to the opposite direction toward the high-energy direction, which is due to the opposite dipole moment directional configuration between the DT and PFDT thiol-molecules. Therefore, the peak shift of XPS would be attributed to surface dipole from the chemisorbed thiol molecules rather than the change in core level of MoS_2.[26] The energy-filtered TEM images at the MoS_2 surface and Raman mapping images also indicate that the thiol-molecules were well adsorbed selectively on the surface of MoS_2 via the vapor-deposition method (Figures S2 and S3, Supporting Information).

To investigate the effect of the thiol-molecules inserted at the contact regions on the electrical characteristics of MoS_2 FETs, especially on the carrier injection properties, we measured the output curves (source–drain current versus source–drain voltage; I_{DS}–V_{DS}) at a fixed gate voltage (V_{GS}) of 40 V for untreated, DT-treated, and PFDT-treated MoS_2 FETs under various temperatures ranging from 80 to 300 K (**Figure 4**a). Note that all the measurements were executed in vacuum (≈10^{-3} Torr) to avoid unwanted effects caused by oxygen and water molecules. For the untreated MoS_2 FETs, I_{DS} increased as temperature increased, whereas that of the thiol-treated MoS_2 FETs was maintained or slightly decreased as temperature increased, as shown in Figure 4a (Figures S3–S7, Supporting Information). Moreover, the output curves of untreated MoS_2 FETs exhibited an obvious *S*-shaped curve at the low V_{DS} regime, which is typically observed if the Schottky contact is formed between a metal electrode and a semiconducting layer. However, the thiol-treated FETs exhibited linear-shaped curves corresponding to the Ohmic contact behaviors even at a low temperature of 80 K. The change in the carrier injection behaviors can be explained by the effect of the inserted thiol-molecules. The carrier injection properties of the untreated MoS_2 FETs were determined by the Schottky barrier as well as a tunneling barrier due to the van der Waals (vdW) gap that is naturally formed between the MoS_2 channel and Au electrode (left panel, Figure 4b).[29,30] Because of the Schottky barrier and tunneling barrier, the

 © 2018 WILEY-VCH Verlag GmbH & Co. KGaA, Weinheim

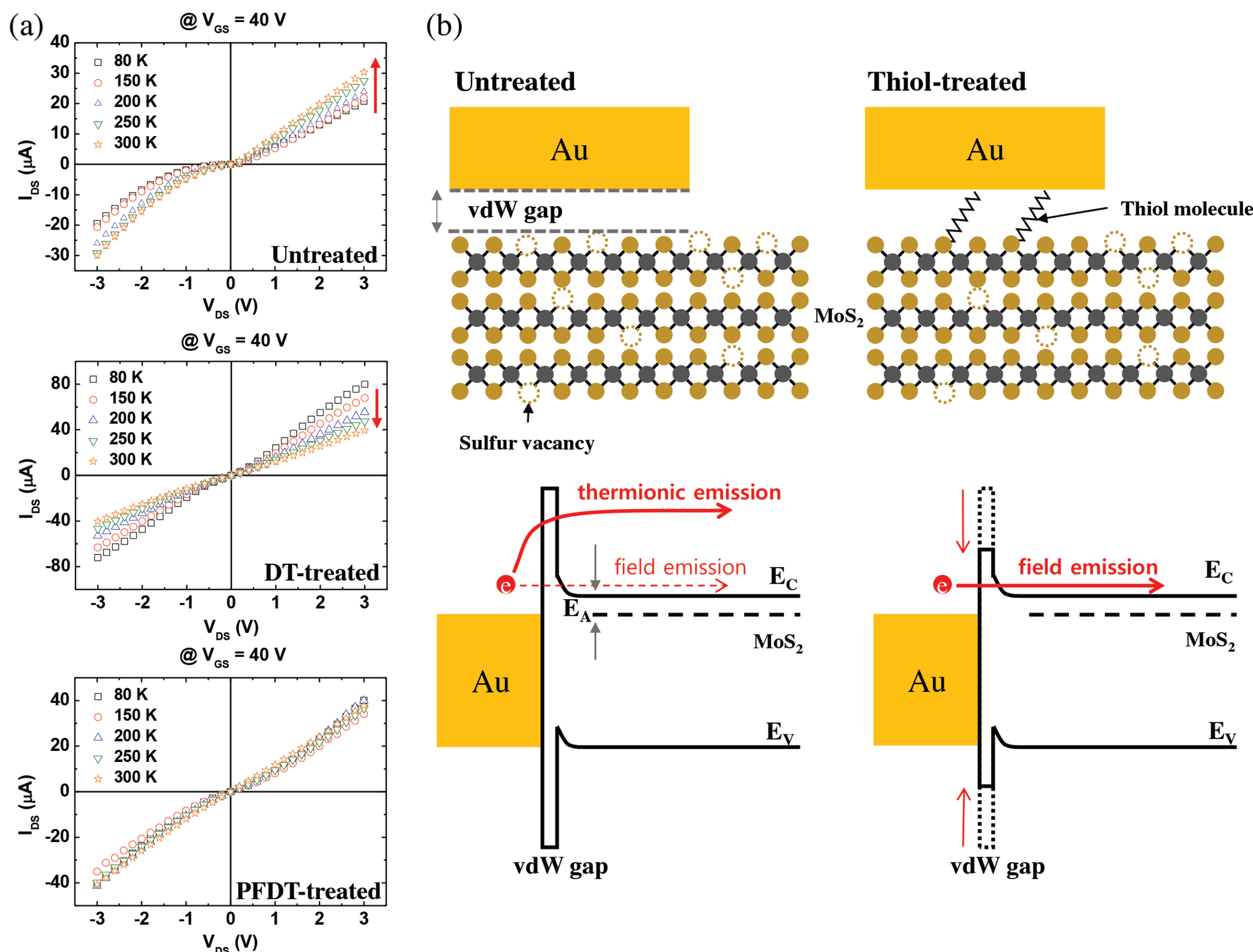

Figure 4. a) Output curves with varying temperature from 80 to 300 K of (top) untreated, (middle) DT-treated, and (bottom) PFDT-treated MoS_2 FETs at fixed gate bias. b) (Top) Contact and (bottom) energy band schematic for (left) untreated and (right) thiol-treated MoS_2.

carriers must have enough activation energy to overcome those barriers to be injected from the metal electrodes to the MoS_2. Consequently, the primary carrier injection mechanism of untreated MoS_2 FETs was thermionic emission resulting in the temperature-dependent I_{DS} and carrier injection behaviors (top panel, Figure 4a). Farmanbar et al. reported that the inserted 2D buffer monolayer layer could interact with the transition metal reducing its work function. Additionally, it can impede the metal-TMDC interaction to remove the interface states (such as sulfur vacancies) which cause the Fermi level pinning, rather than preventing damage from metal evaporation or oxidation due to relatively low coverage of treated thiol molecules.[21,22] Similarly, for the thiol-treated MoS_2 FETs, the adsorbed thiol-molecules could remove the interface states that pinned the Fermi level in the MoS_2 bandgap and create tunneling paths with an effectively lowered barrier at the interface and increased tunneling current through the junction. Therefore, the carriers can be injected more easily from the Au electrode to MoS_2 by field emission (tunneling) with much lower activation energy (bottom panels, Figure 4b). Note that although a slightly decreased I_{DS} was observed due to phonon scattering as the temperature increased, the carrier injection behaviors were insensitive to the temperature. The consistent temperature-dependent behaviors from the V_{DS}–I_{DS} curves were observed in both of the DT-treated MoS_2 FETs without and with the rinsing process (Figure S12, Supporting Information). These results support that the primary carrier-injection mechanism changed from "Schottky-like contact" to "Ohmic-like contact" by inserting thiol-molecules with reduced effective activation energy. In addition, the contact resistance of our devices was evaluated. From the analysis using the Y-function method, the extracted value of contact resistances were found to be ≈35.1, 6.31, and 22.6 kΩ for the untreated device, DT-treated device, and PFDT-treated device, respectively (the detailed explanation is provided in the Supporting Information). The normalized contact resistances considering different device geometry were estimated to be ≈175.5, 25.2, and 67.7 kΩ μm for the untreated device, DT-treated device, and PFDT-treated device, respectively. The contact resistance values of the thiol-treated devices are smaller than those of the untreated devices. By the way, the contact resistance of our untreated device is in agreement with the reported values (10^4–10^5 Ω μm).[30]

© 2018 WILEY-VCH Verlag GmbH & Co. KGaA, Weinheim

Note that sulfur vacancies of MoS_2 can be regarded as a critical factor to determine electrical properties of MoS_2 FETs.[9,31–33] It was reported that pristine MoS_2 has ≈3% of sulfur vacancies.[34] These sulfur vacancies could be donor sites that can increase carrier concentration, resulting in increasing the channel conductance in MoS_2 FET systems.[9,31–33] On the other hand, sulfur vacancies located at contact regions introduce defects levels in the gap, leading to Fermi level pinning.[21,22] In this regards, only multilayer MoS_2 flakes (>20 nm thick) were used as a channel layer to prevent unwanted electrical degradation in this study.[33] And, we introduced thiol-molecules on the sulfur vacancies only at the contact regions, which could eliminate the interfacial states by passivating the sulfur vacancies and create additional tunneling paths through the chemisorbed thiol molecules.

This carrier-injection engineering method enables asymmetric MoS_2 FETs with untreated and DT-treated contact regions by inserting thiol-molecules selectively via the vapor deposition. **Figure 5**a shows the optical images of the MoS_2 devices during the fabrication process to demonstrate asymmetric MoS_2 FETs. First, we fabricated the DT-treated MoS_2 FETs (left panel, Figure 5a). After defining the contact regions using electron-beam lithography, Au S/D electrodes were deposited on the MoS_2 region that was not treated with thiol-molecules (middle panel, Figure 5a). Then, the electrical properties of asymmetric MoS_2 FETs (right panel, Figure 5a) were characterized by measuring the channel current between the untreated and DT-treated contacts in vacuum under various temperatures ranging from 80 to 300 K. Figure 5b shows the output curves of the asymmetric MoS_2 FETs with the DT-treated drain and untreated source electrodes measured at $V_{GS} = 40$ V (black empty symbols) and −20 V (blue filled symbols) at 300 K. At $V_{GS} = 40$ V, symmetric I_{DS} behaviors were exhibited in both the positive and negative V_{DS} regimes (Figure 5b).

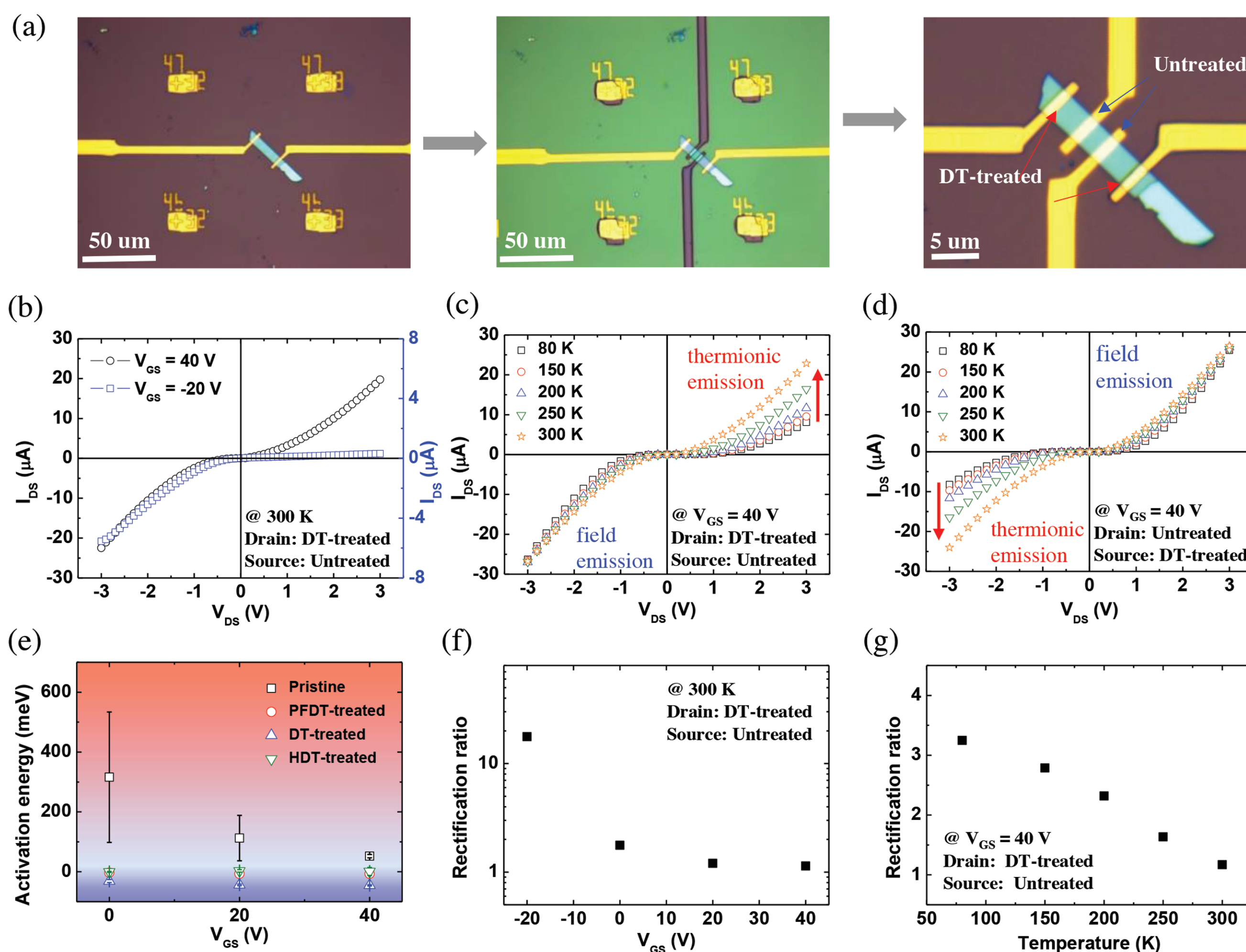

Figure 5. a) Optical images of asymmetric MoS_2 FETs during the fabrication process. b) Output curves at different gate bias conditions at fixed temperature. The drain electrode is DT treated and the source electrode is untreated. c) Output curves at different temperature conditions at a fixed gate bias. The drain electrode is DT treated and the source electrode is untreated. d) Output curves at different temperature conditions at a fixed gate bias. The source electrode is DT treated and the drain electrode is untreated. e) Extracted activation energies of untreated, DT-treated, PFDT-treated, and HDT-treated MoS_2 FETs at different gate bias conditions. Red region represents "thermionic emission dominant" and blue region represents "field emission dominant". f,g) Rectification ratio at V_{DS} of −3 and 3 V in (f) different gate bias conditions at a fixed temperature and at (g) different temperature conditions at a fixed gate bias.

© 2018 WILEY-VCH Verlag GmbH & Co. KGaA, Weinheim

However, at a negative V_{GS} of −20 V, asymmetric I_{DS} behaviors were shown (Figure 5b), which can be explained by the activation energy difference between the untreated and DT-treated contacts. We extracted the activation energy of the untreated and thiol-treated MoS_2 FETs from the output curves using the following equation for thermionic emission in 2D semiconducting system, $I_{DS} = A^* T^{\frac{3}{2}} \exp[(-q/k_B T)(E_A - V_{DS}/\eta)]$ (Figure S9, Supporting Information), where A^*, E_A, and η denote the Richardson coefficient, the effective activation energy, and ideality factor, respectively. From the extracted results, the effective activation energies of thiol-treated MoS_2 FETs were found to be much lower than those of untreated MoS_2 FETs due to the inserted thiol-molecules (Figure 5e). Although DT and PFDT have opposing electric dipole moments, which could affect the work function and Schottky barrier height at the interface between the MoS_2 channel and contacts, both thiol-molecules delivered lowered activation energies regardless of the direction of the electric dipole moments. This result indicates that the thiol-molecules reduced the tunneling barrier with the creation of additional tunneling paths at the contact region, which is more dominant than the effect of their electric dipole moments. A previously reported result by Cheng et al. also supports that both DT and PFDT treatments could improve both the hole and electron injection properties of organic transistors by introducing tunneling paths between the metal electrodes and organic semiconducting layers even though the DT and PFDT have the opposite direction of electric dipole moments.[35] In addition, we applied hexadecanethiol (HDT) molecules, which have 16 carbon chains, on MoS_2 to investigate the effect of the carbon chain length (Figure S7, Supporting Information). For the HDT-treated MoS_2 FETs, a much lower activation energy than that of the untreated MoS_2 FETs was also extracted, but it was slightly higher than those of DT or PFDT-treated MoS_2 FETs because of its longer carbon chain length. It is expected that a similar trend of tunneling behaviors will be observed if shorter molecules than DT are inserted.

For the MoS_2 FETs with the thiol treatment on one contact region, as the gate voltage decreased, the difference of the extracted activation energy increased such that the asymmetric current ratio at −3 and 3 V also increased by ≈20 times (Figure 5e,f). Moreover, while the carrier injection by thermionic emission through the untreated contact was affected by the temperature condition, the carrier injection through the DT-treated contact was insensitive to the temperature (see Figure 5c,d). Therefore, the symmetry in the MoS_2 FETs with the selectively thiol-treated contact region was dependent on the temperature showing an increased asymmetric current ratio as the temperature decreased (Figure 5g). These results were enabled by carrier injection engineering from the thermionic emission to field emission (The details with energy band schematics are described in Figure S10, Supporting Information).

In summary, we introduced thiol-molecules on the contact regions of a MoS_2 semiconductor surface as a tunneling paths to improve contact properties. By conducting a simple vapor treatment on MoS_2 with DT and PFDT molecular solutions, thiol-molecules were successfully chemically adsorbed at the exposed contact regions without physical damage to the electron blocking layer. The thiol-molecules created additional tunneling paths, resulting in a lower energy barrier height between the MoS_2 and metal contacts; therefore, the primary carrier injection mechanism was changed from thermionic emission exhibiting Schottky-contact behaviors to field emission exhibiting Ohmic-contact behaviors. The contact-engineered MoS_2 FETs exhibited much better contact properties with lower activation energies and temperature-insensitive charge injection behaviors. Additionally, by depositing the thiol-molecules on only one contact region in MoS_2 FETs, asymmetric carrier injection was feasible depending on the temperature and the gate bias due to the difference in activation energy. This study presents a high-yield and simple strategy of carrier-injection engineering and can be a promising solution to improve the contact performance in MoS_2 and other 2D semiconductor FET applications.

Experimental Section

MoS_2 FETs Fabrication and Electrical Characterization: MoS_2 was mechanically exfoliated from a MoS_2 bulk crystal (purchased from SPI Supplier, USA) and transferred on SiO_2/p++ Si substrate. PMMA was spin-coated (molecular weight of 4950 k mol^{-1}, 11% dissolved in anisole) with 4000 rpm for 50 s. Then, the substrate was baked at 180 °C for 5 min. In addition, the source and drain electrode patterns were made by using an electron-beam lithography system. After the development process, the substrate was attached on the lid of a 20 mL vial, and 200 µL of thiol molecular solution was transferred into the vial and heated at 70 °C for 3 h in a N_2-filled glove box. Then, the substrate was annealed at 70 °C for 1 h in the N_2-filled glove box to remove residual molecules. After the thiol-molecule deposition, 30 nm thick Au layer was deposited by using an electron beam evaporator. The electrical characteristics of the devices were measured using a semiconductor parameter analyzer (Keithley 4200 SCS) and a temperature variable probe station system (JANIS Model ST-500). Temperature-dependent electrical measurements were conducted varying the temperature from 80 to 300 K using liquid nitrogen.

Characterization of Deposited Thiol-Molecules: EELS data and energy-filtered TEM images were taken by using a HRTEM system (JEM-2100F, JEOL). For the preparation of the MoS_2 samples, a platinum layer as a protective layer for the focused ion beam (Quanta 3D FEG, FEI) was used to prevent carbon contamination. In addition, an XPS (AXIS-SUPRA, KRATOS) mapping image (100 µm × 100 µm) and XPS spectra were obtained to investigate the deposited thiol-molecules. Raman mapping was measured using an XperRam 200 (Nanobase, Inc.) system equipped with a 532 nm laser and a power of 100 µW.

Supporting Information

Supporting Information is available from the Wiley Online Library or from the author.

Acknowledgements

The authors appreciate the financial support of the National Creative Research Laboratory program (Grant No. 2012026372) through the National Research Foundation of Korea (NRF), funded by the Korean Ministry of Science and ICT. S.C appreciates the support by the National Research Foundation of Korea (NRF) grant funded by the Korea government (MSIP; Ministry of Science, ICT & Future Planning) (NRF-2017R1C1B2002323).

© 2018 WILEY-VCH Verlag GmbH & Co. KGaA, Weinheim

Conflict of Interest

The authors declare no conflict of interest.

Keywords

charge injection, contact engineering, electrical transport, MoS_2, thiol-molecules

Received: September 25, 2017
Revised: January 29, 2018
Published online: March 23, 2018

[1] B. Radisavljevic, A. Radenovic, J. Brivio, V. Giacometti, A. Kis, *Nat. Nanotechnol.* **2011**, *6*, 147.
[2] Q. H. Wang, K. Kalantar-Zadeh, A. Kis, J. N. Coleman, M. S. Strano, *Nat. Nanotechnol.* **2012**, *7*, 699.
[3] K. F. Mak, C. Lee, J. Hone, J. Shan, T. F. Heinz, *Phys. Rev. Lett.* **2010**, *105*, 136805.
[4] D. Xiao, G.-B. Liu, W. Feng, X. Xu, W. Yao, *Phys. Rev. Lett.* **2012**, *108*, 196802.
[5] Y. Yoon, K. Ganapathi, S. Salahuddin, *Nano Lett.* **2011**, *11*, 3768.
[6] D. Jariwala, V. K. Sangwan, L. J. Lauhon, T. J. Marks, M. C. Hersam, *ACS Nano* **2014**, *8*, 1102.
[7] Y. Zhan, Z. Liu, S. Najmaei, P. M. Ajayan, J. Lou, *Small* **2012**, *8*, 966.
[8] C.-H. Lee, G.-H. Lee, A. M. v. d. Zande, W. Chen, Y. Li, M. Han, X. Cui, G. Arefe, C. Nuckolls, T. F. Heinz, J. Guo, J. Hone, P. Kim, *Nat. Nanotechnol.* **2014**, *9*, 676.
[9] M. Amani, D.-H. Lien, D. Kiriya, J. Xiao, A. Azcatl, J. Noh, S. R. Madhvapathy, R. Addou, S. KC, M. Dubey, K. Cho, R. M. Wallace, S.-C. Lee, J.-H. He, J. W. Ager III, X. Zhang, E. Yablonovitch, A. Javey, *Science* **2015**, *350*, 1065.
[10] D. Jena, K. Banerjee, G. H. Xing, *Nat. Mater.* **2014**, *13*, 1076.
[11] J. Wang, Q. Yao, C.-W. Huang, X. Zou, L. Liao, S. Chen, Z. Fan, K. Zhang, W. Wu, X. Xiao, C. Jiang, W.-W. Wu, *Adv. Mater.* **2016**, *28*, 8302.
[12] X. Cui, E.-M. Shin, L. A. Jauregui, S. H. Chae, Y. D. Kim, B. Li, D. Seo, K. Pistunova, J. Yin, J.-H. Park, H.-J. Choi, Y. H. Lee, K. Watanabe, T. Taniguchi, P. Kim, C. R. Dean, J. C. Hone, *Nano Lett.* **2017**, *17*, 4781.
[13] H. Kwon, W. Choi, D. Lee, Y. Lee, J. Kwon, B. Yoo, C. P. Grigoropoulos, S. Kim, *Nano Res.* **2014**, *7*, 1137.
[14] R. Kappera, D. Voiry, S. E. Yalcin, B. Branch, G. Gupta, A. D. Mohite, M. Chhowalla, *Nat. Mater.* **2014**, *13*, 1128.
[15] X. Cui, G.-H. Lee, Y. D. Kim, G. Arefe, P. Y. Huang, C.-H. Lee, D. A. Chenet, X. Zhang, L. Wang, F. Ye, F. Pizzocchero, B. S. Jessen, K. Watanabe, T. Taniguchi, D. A. Muller, T. Low, P. Kim, J. Hone, *Nat. Nanotechnol.* **2015**, *10*, 534.
[16] L. Yu, Y.-H. Lee, X. Ling, E. J. G. Santos, Y. C. Shin, Y. Lin, M. Dubey, E. Kaxiras, J. Kong, H. Wang, T. Palacios, *Nano Lett.* **2014**, *14*, 3055.
[17] S. Das, H.-Y. Chen, A. V. Penumatcha, J. Appenzeller, *Nano Lett.* **2012**, *13*, 100.
[18] J. Kang, W. Liu, K. Banerjee, *Appl. Phys. Lett.* **2014**, *104*, 093106.
[19] X. Duan, C. Wang, A. Pan, R. Yu, X. Duan, *Chem. Soc. Rev.* **2015**, *44*, 8859.
[20] C. Huang, S. Wu, A. M. Sanchez, J. J. P. Peters, R. Beanland, J. S. Ross, P. Rivera, W. Yao, D. H. Cobden, X. Xu, *Nat. Mater.* **2014**, *13*, 1096.
[21] M. Farmanbar, G. Brocks, *Phys. Rev. B* **2015**, *91*, 161304.
[22] M. Farmanbar, G. Brocks, *Adv. Electron. Mater.* **2016**, *2*, 1500405.
[23] M. Makarova, Y. Okawa, M. Aono, *J. Phys. Chem. C* **2012**, *116*, 22411.
[24] C. G. Wiegenstein, K. H. Schulz, *J. Phys. Chem. B* **1999**, *103*, 6913.
[25] S. L. Peterson, K. H. Schulz, *Langmuir* **1996**, *12*, 941.
[26] X. Chen, N. C. Berner, C. Backes, G. S. Duesberg, A. R. McDonald, *Angew. Chem.* **2016**, *55*, 5803.
[27] D. M. Sim, M. Kim, S. Yim, M.-J. Choi, J. Choi, S. Yoo, Y. S. Jung, *ACS Nano* **2015**, *9*, 12115.
[28] S. Bertolazzi, S. Bonacchi, G. Nan, A. Pershin, D. Beljonne, P. Samori, *Adv. Mater.* **2017**, *29*, 1606760.
[29] J. Kang, W. Liu, D. Sarkar, D. Jena, K. Banerjee, *Phys. Rev. X* **2014**, *4*, 031005.
[30] A. Allain, J. Kang, K. Banerjee, A. Kis, *Nat. Mater.* **2015**, *14*, 1195.
[31] X. Zhang, Q. Liao, S. Liu, Z. Kang, Z. Zhang, J. Du, F. Li, S. Zhang, J. Xiao, B. Liu, Y. Ou, X. Liu, L. Gu, Y. Zhang, *Nat. Commun.* **2017**, *8*, 15881.
[32] H. Qiu, T. Xu, Z. Wang, W. Ren, H. Nan, Z. Ni, Q. Chen, S. Yuan, F. Miao, F. Song, G. Long, Y. Shi, L. Sun, J. Wang, X. Wang, *Nat. Commun.* **2013**, *4*, 2642.
[33] K. Cho, M. Min, T.-Y. Kim, H. Jeong, J. Pak, J.-K. Kim, J. Jang, S. J. Yun, Y. H. Lee, W.-K. Hong, T. Lee, *ACS Nano* **2015**, *9*, 8044.
[34] C. Tsai, H. Li, S. Park, J. Park, H. S. Han, J. K. Nørskov, X. Zheng, F. Abild-Pedersen, *Nat. Commun.* **2017**, *8*, 15113.
[35] X. Cheng, Y.-Y. Noh, J. Wang, M. Tello, J. Frisch, R.-P. Blum, A. Vollmer, J. P. Rabe, N. Koch, H. Sirringhaus, *Adv. Funct. Mater.* **2009**, *19*, 2407.

© 2018 WILEY-VCH Verlag GmbH & Co. KGaA, Weinheim